Nature geoscience
April 2015, Volume 8, Issue 4, Pages 299-304
http://dx.doi.org/10.1038/ngeo2387
http://archimer.ifremer.fr/doc/00255/36658/

Presence of oxygen and aerobic communities from sea floor to basement in deep-sea sediments

D'Hondt Steven [1] [*], Inagaki Fumio [2], Alvarez Zarikian Carlos [3], Abrams Lewis J. [4], Dubois Nathalie [5], Engelhardt Tim [6], Evans Helen [3], Ferdelman Timothy [7], Gribsholt Britta [8], Harris Robert N. [9], Hoppie Bryce W. [10], Hyun Jung-Ho [11], Kallmeyer Jens [12], Kim Jinwook [13], Lynch Jill E. [14], Mckinley Claire C. [15], Mitsunobu Satoshi [16], Morono Yuki [2], Murray Richard W. [17], Pockalny Robert [1], Sauvage Justine [1], Shimono Takaya [18], Shiraishi Fumito [19], Smith David C. [1], Smith Duke Christopher E. [20], Spivack Arthur J. [1], Steinsbu Bjorn Olav [21], Suzuki Yohey [22], Szpak Michal [23], Toffin Laurent [24], Uramoto Goichiro [2], Yamaguchi Yasuhiko T. [22], Zhang Guo-Liang [25], Zhang Xiao-Hua [26], Ziebis Wiebke [27]

[1] Graduate School of Oceanography, University of Rhode Island, 215 South Ferry Road Narragansett, Rhode Island 02882, USA
[2] Kochi Institute for Core Sample Research, Japan Agency for Marine-Earth Science and Technology, Monobe B200, Nankoku Kochi 783-8502, Japan
[3] International Ocean Discovery Program, Texas A&M University, 1000 Discovery Drive, College Station Texas 77845-9547, USA
[4] Center for Marine Science, University of North Carolina at Wilmington, 5600 Marvin K. Moss Lane Wilmington, North Carolina 28409, USA
[5] Swiss Federal Institute of Aquatic Science and Technology, Ueberlandstrasse 133 8600 Duebendorf, Switzerland
[6] Institut für Chemie und Biologie Des Meeres, Carl von Ossietzky Universität Oldenburg, Oldenburg 26129, Germany
[7] Department of Biogeochemistry, Max-Planck-Institute of Marine Microbiology, Celsiusstrasse 1, 28359 Bremen, Germany
[8] Center for Geomicrobiology, Aarhus Universitet, Ny Munkegade 114, Building 1540 8000 Aarhus, Denmark
[9] College of Earth, Oceanic, and Atmospheric Sciences, Oregon State University, 104 COAS Admin Building Corvallis, Oregon 97331-5503, USA
[10] Minnesota State University, Mankato, Department of Chemistry and Geology, Ford Hall 241, Mankato Minnesota 56001, USA
[11] Department of Marine Sciences and Convergent Technology, Hanyang University, 1271 Sa-3 dong, Ansan Gyeonggi-do 426-791, Korea
[12] GFZ German Research Centre for Geosciences, Section 4.5 Geomicrobiology, Telegrafenberg, 14473 Potsdam, Germany
[13] Earth Systems Sciences, Yonsei University, 134 Shinchon dong 120-749 Seoul, Korea
[14] School of Earth Sciences, University of Melbourne, McCoy Building Melbourne, Victoria 3010, Australia
[15] Department of Oceanography, Texas A&M University, College Station Texas 77843, USA
[16] Institute for Environmental Sciences, Shizuoka University, 52-1 Yada Suruuga-ku, Shizuoka 422-8526, Japan
[17] Department of Earth and Environment, Boston University, 675 Commonwealth Avenue Boston, Massachusetts 02215, USA
[18] Graduate School of Life and Environmental Sciences, University of Tsukuba, 1-1-1 Tennoudai

Tsukuba, Ibaraki 305-8572, Japan
[19] Graduate School of Science, Hiroshima University, 1-3-1 Kagamiyama, Higashi-Hiroshima Hiroshima 739-8526, Japan
[20] National Oceanography Centre, University of Southampton, European Way Southampton SO14 3ZH, UK
[21] Department of Earth Science, University of Bergen, Allegaten 41 5007 Bergen, Norway
[22] Earth and Planetary Science Department, Graduate School of Science, The University of Tokyo, 7-3-1 Hongo Bunkyo-ku, Tokyo 113-0033, Japan
[23] School of Chemical Sciences, Dublin City University, Collins Avenue Glasnevin, Dublin 9, Ireland
[24] Institut Français de Recherche pour l'Exploitation de la Mer, Centre Bretagne, CS 10070 29280 Plouzané, France
[25] South China Sea Institute of Oceanology, Chinese Academy of Sciences, 7 Nanhai Road, Shinan Region Qingdao 266071, China
[26] College of Marine Life Sciences, Ocean University of China, 5 Yushan Road Qingdao 266003, China
[27] Department of Biological Sciences, University of Southern California, 3616 Trousdale Boulevard, AHF 335 Los Angeles, California 90089, USA

* Corresponding author : Steven D'Hondt, email address : dhondt@mail.uri.edu

---

Abstract :

The depth of oxygen penetration into marine sediments differs considerably from one region to another. In areas with high rates of microbial respiration, O2 penetrates only millimetres to centimetres into the sediments, but active anaerobic microbial communities are present in sediments hundreds of metres or more below the sea floor. In areas with low sedimentary respiration, O2 penetrates much deeper but the depth to which microbial communities persist was previously unknown. The sediments underlying the South Pacific Gyre exhibit extremely low areal rates of respiration. Here we show that, in this region, microbial cells and aerobic respiration persist through the entire sediment sequence to depths of at least 75 metres below sea floor. Based on the Redfield stoichiometry of dissolved O2 and nitrate, we suggest that net aerobic respiration in these sediments is coupled to oxidation of marine organic matter. We identify a relationship of O2 penetration depth to sedimentation rate and sediment thickness. Extrapolating this relationship, we suggest that oxygen and aerobic communities may occur throughout the entire sediment sequence in 15–44% of the Pacific and 9–37% of the global sea floor. Subduction of the sediment and basalt from these regions is a source of oxidized material to the mantle.

Main

Morita and ZoBell nearly 60 years ago reported "the lower limits of the biosphere" at 3.9 to 7.5 meters below seafloor (mbsf) in abyssal clay of the oligotrophic North Pacific Gyre (NPG)[17]. Recent studies pushed the lower limit of the known sedimentary biosphere to slightly greater depths in abyssal clay of oligotrophic regions; microbial cells have been identified at 8 mbsf in the ultra-oligotrophic South Pacific Gyre (SPG)5 and 20 mbsf in the NPG6, and aerobic respiration has been inferred to nearly 30 mbsf in the NPG6. However, the existence, nature and consequences of life at greater sedimentary depths in the oligotrophic ocean have remained unknown.

To document the nature of life and habitability in the deepest abyssal sediment of a major low-productivity oceanic region, we undertook Integrated Ocean Drilling Program (IODP) Expedition 329 to the South Pacific Gyre (Oct-Dec 2010)7. The SPG is Earth's largest oligotrophic ocean region, covering ~10% of Earth's surface. Oxygen flux across the SPG seafloor is extremely low[18]. Mean sedimentation rate, surface chlorophyll concentrations and primary productivity are lower in the SPG than in any other oceanic region5. Shallow cores in abyssal sediment of the SPG exhibit the lowest seafloor cell concentrations and the lowest areal

rates of microbial activity ever previously encountered in marine sediment[5, 19].

Six of the seven Expedition 329 sites are located in the low-chlorophyll SPG (U1365-U1370), and one is located in the more biologically productive region south of the SPG (U1371) (Fig 1)[7]. These sites range in water depth from 3740 meters below sea level (mbsl) (U1368) to 5695 mbsl (U1365) (SI). Sediment temperature (1.1°-10.6° C) is habitable by psychrophiles at all sites[7]. Basement age ranges from 13.5 Ma (U1368) to 84-120 Ma (U1365 and U1366) (SI). Sediment thickness co-varies with basement age and is lower at the SPG sites (16 - 75 m) than at Site U1371 south of the SPG (131 m)[7]. Site U1370 migrated into the gyre from the southern biologically productive region between 20 and 30 myrs ago (Fig 1)[7]. The other sites have resided within the low-chlorophyll region for most or all of their history.

Microbial cells are present throughout the entire sediment sequence at all seven sites. At the six SPG sites (U1365-U1370), cell counts are extremely low and decrease with increasing sediment depth (Fig 2). They are one to seven orders of magnitude lower than counts at the same depths in previously drilled sites of ocean margins and upwelling regions[19]. They are up to two orders of magnitude lower than cell counts in piston-cored sediment of the oligotrophic NPG[19]. Site U1371, in the higher productivity region south of the gyre, is characterized by cell counts that are generally higher than at the SPG sites between 0 and 40 mbsf (Fig 2); at greater depths, they converge with the SPG counts.

At the six sites within the SPG, dissolved O_2 is present from the seafloor to the sediment-basement interface (Fig 2)[7]. Dissolved O_2 persists even in the deepest sediment at U1365 (62 to 75 mbsf) despite an intervening ~20-m layer of chert[7]. Persistence of dissolved O_2 throughout the SPG sediment sequence is consistent with the much earlier discovery that dissolved nitrate (NO_3^-) is at or above deep-water concentrations throughout the entire sediment column of Deep

55 Sea Drilling Project Leg 92 sites elsewhere in the SPG[20] (NO_3^- reduction does not occur until
56 most or all O_2 is depleted[21]). Because dissolved O_2 is present in the deepest sediment, it must
57 also be present in the basement aquifer in diffusive contact with this sediment. This discovery[7]
58 greatly expands the subsurface envelope of the oxic realm to include the entire sedimentary
59 sequence and the upper basaltic basement throughout the entire SPG.
60 In oceanic regions where dissolved O_2 penetrates only mm to decimeters into the sediment,
61 the sediment is exposed to O_2 for a very short time (years to kyrs) before it enters a deep anoxic
62 realm[22]. In contrast, SPG sediment is exposed to dissolved O_2 for an extraordinarily long time,
63 and never becomes anoxic. Because O_2 penetrates the entire sedimentary sequence, O_2 exposure
64 time for SPG sediment is formally equal to the age of the oldest sediment at each site, implying
65 that SPG sediment is continuously exposed to O_2 for its entire history (up to 120 myrs at Site
66 U1365) (SI).
67 In comparison, dissolved O_2 is absent from most of the sediment column at U1371, in the
68 moderately productive subtropical convergence south of the SPG (Fig 1)[7]. At this site, O_2
69 diffusing down from the ocean decreases below detection within 0.9 mbsf and traces of O_2
70 penetrate ~15 meters upward into the sediment from the underlying basaltic aquifer. Oxygen
71 exposure time for the shallow sediment at U1371 is only 35 kyrs (SI).
72 The presence of dissolved O_2, nitrate (NO_3^-), phosphate (PO_4^-) and dissolved inorganic
73 carbon (DIC = CO_3^{2-} + HCO_3^- + CO_2) throughout the sediment of SPG sites U1365-U1370 (Fig
74 2)[7] indicates that cell abundance and metabolic activity are not limited by availability of electron
75 acceptors or dissolved major inorganic nutrients (C, N, P) in the sediment or the upper basaltic
76 basement. Concentration profiles of the dissolved metabolic products PO_4^-, DIC, and, at Site
77 U1370, NO_3^- exhibit more complexity than dissolved O_2 profiles and the other NO_3^- profiles,

78 because DIC and, at U1370, NO_3^- are affected by loss to the basement and PO_4^- and DIC interact
79 with sedimentary minerals.
80 Dissolved NO_3^- is produced in the sediment by aerobic degradation and subsequent
81 nitrification of nitrogen from buried organic matter[21]. Downhole changes in dissolved NO_3^- and
82 O_2 concentrations closely match the Redfield NO_3^-:O_2 ratio (16:-170)[23], suggesting that net O_2
83 reduction is almost solely due to oxidation of buried organic matter (SI).
84 Analysis of undisturbed coring intervals indicates that net O_2 reduction occurs throughout the
85 entire sedimentary sequence at very low rates (Fig 3) (SI). Net O_2 consumption is highest in the
86 first 1.1 to 2.3 mbsf of the SPG sites, ranging from $6.3*10^{-11}$ moles $O_2/cm^3/yr$ at U1366 to
87 $5.3*10^{-10}$ moles/cm^3/yr at U1367 (Fig 3). These rates are considerably lower than rates reported
88 from equivalent depths in sediment of the oligotrophic NPG (10^{-7} moles $O_2/cm^3/yr$)[6]. With
89 increasing depth, the rate of net O_2 consumption rapidly decreases to even lower values. It is
90 generally indistinguishable from zero in zones that span intervals of drilling disturbance (Fig 3).
91 In the undisturbed sediment, net O_2 consumption rates are generally distinguishable from zero
92 and range from $3.3*10^{-13}$ moles $O_2/cm^3/yr$ at U1370 (37.5 to 68 mbsf) to $1.5*10^{-11}$ moles
93 $O_2/cm^3/yr$ at U1365 (4.9 to 8.8 mbsf) (Fig 3) (SI).
94 Within the SPG, depth-integrated subseafloor net O_2 reduction rates (from 1.5 mbsf to
95 sediment-basalt interface) decrease from gyre edge to gyre center, in parallel with seasurface
96 chlorophyll content (SI). Peak concentrations of dissolved PO_4^-, DIC and TOC are also
97 consistent with organic-fueled subseafloor respiration declining from outside the gyre (U1371) to
98 gyre center (U1368) (Fig 2).
99 Gross rates of O_2 consumption presumably exceed these organic-fueled rates of net O_2
100 reduction, because in situ water radiolysis generates both H_2 and O_2 in marine sediment[24] and

most H_2 produced in SPG sediment is quickly consumed (concentrations of dissolved H_2 at these sites are generally below 1 nM and never exceed 90 nM)[7] (SI). The Redfield stoichiometry of O_2 reduction to NO_3^- production in SPG sediment suggests that radiolytic production of O_2 does not significantly contribute to the dissolved O_2 concentrations (perhaps because H_2 is kept at low concentrations by reactions that reverse radiolytic production of H_2, O_2 and H_2O_2, such as the microbially mediated Knallgas reaction).

Mean organic-fueled respiration per cell in the shallowest SPG sediment (1.6-2.3 mbsf) is in the range of $1.2*10^{-15}$ moles e^-/cell/year (U1365) to $1.1*10^{-14}$ moles e^-/cell/year (U1366). Mean organic-fueled per-cell respiration is generally even lower at greater depths; in intervals where the volumetric O_2 consumption rate is distinguishable from zero, mean organic-fueled per-cell respiration is between $3.2*10^{-17}$ moles e^-/cell/year and $6.8*10^{-14}$ moles e^-/cell/year. These rates at greater depths overlap with mean per-cell respiration rates reported for deep subseafloor aerobes in the North Pacific Gyre ($1.5*10^{-15}$ moles e^-/cell/year)[6]. The rates from SPG depths where O_2 consumption is distinguishable from zero generally exceed mean per-cell rates of deep subseafloor anaerobes in eastern equatorial Pacific sediment [$2.8*10^{-18}$ to $1.7*10^{-17}$ moles e^-/cell/year (SI)].

These per-cell rates of organic-fueled respiration are broadly consistent with the general interpretation that microbial respiration rates are extraordinarily low in subseafloor sediment[25, 5, 6, 13, 16]. Nevertheless, estimates of per-cell rates must be treated with caution for the following reasons: (i) the ratio of active cells to dead or moribund cells in counted populations is not yet known, and (ii) the contribution of radiolytic H_2 oxidiation to microbial respiration in SPG sediment is also unknown.

The primary driver of the reductions in cell abundance and net (organic-fueled) O_2 reduction

124 with increasing sediment depth at SPG sites (U1365-U1370) appears to be decreasing
125 availability of organic matter with increasing sediment age. Total organic carbon (TOC) content
126 decreases rapidly with sediment depth, from values between 0.08% (U1368) and 0.25% (U1370)
127 in the first centimeters below seafloor to stable values of "below detection" (0.002%) to 0.03% at
128 greater depths (Fig 2). This decrease in TOC with increasing depth is primarily due to
129 consumption within the sediment; as the sediment ages, less TOC remains to be consumed[26].
130 Total organic carbon approaches our detection limit deep in the sediment at all six SPG sites,
131 including U1370 (Fig 2), which migrated through the higher productivity region south of the
132 SPG early in its history (Fig 1). In comparison, TOC is greater than 0.1% through the upper 100
133 mbsf at Site U1371 (south of the SPG) and greater than 1.0% for hundreds of mbsf at some
134 ocean-margin sites[27].
135 Depth of O_2 penetration ultimately depends on the balance between supply of reduced
136 oxidizable material (primarily organic matter) and supply of dissolved O_2[1]. In near-seafloor
137 sediment, organic flux to the seafloor exerts primary control[28]. The situation becomes more
138 complicated as sediment depth and age increase, because (i) the supply of organic matter at depth
139 in sediment depends on both the initial flux of reduced material to the seafloor and the
140 subsequent oxidation history of that material at successively greater sediment depths, and (ii) the
141 timescale required for diffusion (e.g., of dissolved O_2) depends on the square of the distance
142 penetrated[29].
143 Comparison of our SPG results to other sites indicate that dissolved O_2 penetrates the entire
144 sediment column at sites with low mean sediment accumulation rates and relatively thin
145 sediment thickness (Fig 4) (SI). This result is consistent with the complexities outlined above.
146 Dependence of O_2 penetration depth on sediment accumulation rate is consistent with depth of

147 O_2 penetration depending on organic burial rate; organic flux to the seafloor broadly co-varies
148 with sedimentation rate[18] and at very low sediment accumulation rates, most organic matter is
149 consumed at or near the seafloor and very little remains to be buried[30, 6]. Dependence of O_2
150 penetration depth on sediment thickness is consistent with the exponential effect of diffusive
151 distance on diffusive timescale; as sediment thickness increases, O_2 disappears faster than it can
152 diffuse to the greatest depths.
153 Our results have significant implications for the nature and global distribution of subseafloor
154 life. The persistence of microbial cells and aerobic respiration throughout the entire sediment
155 sequence indicates that there is no depth limit to the biosphere within the sediment of the most
156 oligotrophic ocean region. If active microbial communities and O_2 penetrate to basement
157 throughout the regions shown in figure 4, an aerobic ecosystem is present throughout the
158 sediment column and the upper basement over 15-44% of the Pacific seafloor and 9-37% of the
159 entire ocean (Fig 4) (SI).
160 Throughout this vast area of O_2 penetration to basement, the predominant microbial activities
161 are aerobic throughout the sediment column, subseafloor rates of organic-fueled respiration and
162 cell abundances are extremely low, and sedimentary oxygen exposure time equals basement age.
163 This large-scale pattern of subseafloor oxidation may ultimately affect the chemical
164 evolution of Earth's mantle and subduction-related volcanic systems. In subduction zones where
165 deep sediment and basalt of the sinking slab became anoxic early in their history, the principal
166 redox species in the upper portion of the sinking slab include reduced iron, reduced sulfur and
167 reduced organic carbon[31]. In contrast, in subduction zones where dissolved O_2 penetrates (or long
168 penetrated) the sediment sequence and the upper basement (e.g., the Tonga Trench and the Peru-
169 Chile Trench), oxidized iron and manganese are abundant and reduced metal, reduced sulfur and

reduced organic matter are largely absent in the upper portion of the sinking slab (SI). The redox state of subducted material influences the extent of mantle oxidation[32], which in turn affects magmatic evolution, mineral assemblage and gas speciation in volcanic systems, and the long-term evolution of atmospheric oxygen content[31].

References

[1] Emerson, S., K. Fischer, K., Reimers C., & Heggie, D. Organic carbon dynamics and preservation in deep-sea sediments. *Deep-Sea Res*. **32**, 1-21 (1985).

[2] Jahnke, R.A., Heggie, D., Emerson, S. & Grundmanis, V. Pore waters of the central Pacific Ocean: Nutrient results. *Earth Planet. Sci. Lett.* **61**, 233-256 (1982).

[3] Revsbech, N. P., Jørgensen, B. B. & Blackburn, T. H. Oxygen in the sea bottom measured with a microelectrode. *Science* **207**, 1355-1356 (1980).

[4] Murray, J. W. & Grundmanis, V. Oxygen consumption in pelagic marine sediments. *Science* **209**, 1527-1530 (1980).

[5] D'Hondt, S. *et al.* Subseafloor sedimentary life in the South Pacific Gyre. *Proc. Nat. Acad. Sci. U.S.A.* **106**, 11651-11656, doi:10.1073/pnas.0811793106 (2009).

[6] Røy, H., Kallmeyer, J., Adhikari, R. R., Pockalny, R., Jørgensen, B. B. & D'Hondt, S. Aerobic microbial respiration in 86-million-year-old deep-sea red clay, *Science* **336** (6083), 922-925, DOI: 10.1126/science.1219424 (2012).

[7] D'Hondt, S., Inagaki, F., Alvarez Zarikian, C.A., and the Expedition 329 Scientists. *Proc. IODP,* 329: Tokyo (Integrated Ocean Drilling Program Management International, Inc.), doi:10.2204/ iodp.proc.329.2011 (2011).

[8] Orcutt, B. N. *et al*., Oxygen consumption rates in subseafloor basaltic crust derived from a reaction transport model, *Nat. Commun.* **4**, 2539, DOI: 10.1038/ncomms3539 (2013).

[9] Whelan, J. K. *et al*. Evidence for sulfate-reducing and methane-producing microorganisms in sediments from Sites 618, 619 and 622, in *Init. Repts. DSDP* **96** (eds. Bouma, A. H., Coleman, J. M., Meyer, A. W., et al.), 767-775 (U.S. Government Printing Office, Washington D.C., 1986).

198 [10] Parkes, R. J. *et al.* Deep bacterial biosphere in Pacific Ocean sediments. *Nature* **371**, 410-
199 413 (1994).
200 [11] Head, I. M., Jones, D. M. & Larter, S. R. Biological activity in the deep subsurface and
201 the origin of heavy oil, *Nature* **626**(6964), 344-352 (2003).
202 [12] D'Hondt, S. *et al.* Distributions of microbial activities in deep subseafloor sediments.
203 *Science* **306**, 2216-2221 (2004).
204 [13] Schippers, A. *et al.* Prokaryotic cells of the deep sub-seafloor biosphere identified as
205 living bacteria. *Nature* **433**, 861-864 (2005).
206 [14] Inagaki, F. *et al.* Biogeographical distribution and diversity of microbes in methane
207 hydrate-bearing deep marine sediments, on the Pacific Ocean Margin. *Proc. Nat. Acad.*
208 *Sci. U.S.A.* **103**, 2815-2820 (2006).
209 [15] Batzke, A., Engelen, B., Sass, H. & Cypionka, H. Phylogenetic and physiological
210 diversity of cultured deep-biosphere bacteria from Equatorial Pacific Ocean and Peru
211 Margin Sediments. *Geomicrobiol. J.* **24**, 261-273 (2007).
212 [16] Lomstein, B.A., Langerhuus, A.T., D'Hondt, S., Jørgensen, B.B. & Spivack, A.J. Spore
213 abundance, microbial growth and necromass turnover in deep subseafloor sediment,
214 *Nature* **484**, 101–104 (2012).
215 [17] Morita, R.Y. & Zobell, C.E., Occurrence of bacteria collected during the Mid-Pacific
216 Expedition, Deep-Sea Research 3, 66-73 (1955).
217 [18] Jahnke, R. A. The global ocean flux of particulate organic carbon: areal distribution
218 and magnitude. *Global Biogeochem. Cycles* **10**, 71-88 (1996).
219 [19] Kallmeyer, J., Pockalny, R. Adhikari, R., Smith D. C. & D'Hondt, S. Global distribution
220 of subseafloor sedimentary biomass, *Proc. Nat. Acad. Sci. U.S.A.* **109**, 16213-16216

(2012).

[20] Gieskes, J. M. & Boulegue, J. Interstitial Water Studies, Leg-92, *Initial Reports of the Deep Sea Drilling Project* **92**, 423-429 (1986).

[21] Hensen, C. & Zabel, M. Early Diagenesis at the Benthic Boundary Layer: Oxygen and Nitrate in Marine Sediments, in *Marine Geochemistry* (eds. Schulz, H. D. & Zabel, M.), Springer-Verlag (Berlin), 209-231 (2000).

[22] Hedges, J.I., F.S. Hu, A.H. Devol, H.E. Hartnett, E. Tsamakis & R.G. Keil, Sedimentary organic matter preservation: a test for selective degradation under oxic conditions, *Am. J. Sci.* **299**, 529-555 (1999).

[23] Anderson, L. A. & Sarmiento, J. L. Global ocean phosphate and oxygen simulations. *Glob. Biogeochem. Cy.* **9**, 621-636 (1995).

[24] Blair, C. C., D'Hondt, S., Spivack, A. J. & Kingsley, R. H. Potential of radiolytic hydrogen for microbial respiration in subseafloor sediments, *Astrobiol.* **7**(6), 951-970 (2007).

[25] D'Hondt, S., Rutherford, S. & Spivack, A. J. Metabolic activity of subsurface life in deep-sea sediments, *Science* **295**, 2067-2070 (2002).

[26] Middelburg, J.J., A simple rate model for organic matter decomposition in marine sediments, *Geochim. Cosmochim. Ac.* **53**, 1577-1581 (1989).

[27] Meister, P., Prokopenko, M., Skilbeck, C. G., Watson, M. & McKenzie, J. in *Proc. ODP, Sci. Results* **201** (eds S.L. D'Hondt, B.B. Jørgensen, & D.J. Miller) (2005).

[28] Murray, J.W. & Kuivila, K.M. Organic matter diagenesis in the northeast Pacific: Transition from aerobic red clay to suboxic hemipelagic sediments. *Deep Sea Res.* **37**, 59-80 (1990).

[29] Einstein, A., Über die von der molekularkinetischen Theorie der Wärme geforderte Bewegung von in ruhenden Flüssigkeiten suspendierten Teilchen, *Annalen der Physik* **17** (8), 549–560 (1905). English translation by A.D. Cowper (1926): Investigations on the theory of Brownian movement.

[30] Heath, G. R., Moore, T. C. Jr. & Dauphin, J. P. Organic Carbon in Deep-Sea Sediments, in *The Fate of Fossil Fuel CO_2 in the Oceans* (eds. Andersen, N. R. & Malahoff, A.), Plenum Press, New York, 605-625 (1977).

[31] Evans, K.A., The redox budget of subduction zones, *Earth-Sci. Rev.* **113**, 11-32 (2012).

[32] Kelley, K. A. and E. Cottrell, Water and the Oxidation State of Subduction Zone Magmas; *Science* **325** (5940): 605-607 (2009).

[33] Laske G. and G.A. Masters, global digital map of sediment thickness. *EOS Trans. AGU,* 78:F483 (1997).

[34] Divins D.L., NGDC Total Sediment Thickness of the World's Oceans & Marginal Seas, (NOAA) (2008).

Supplementary Information is linked to the online version of the paper at www.nature.com/nature.

Acknowledgments. This research would not have been possible without the dedicated effort of the drilling crew, ship's crew and scientific staff of the Drillship *JOIDES Resolution*. We thank Victoria M. Fulfer and Maureen J. Hayden for assistance with data compilation. The project was undertaken as part of Integrated Ocean Drilling Program Expedition (IODP) 329. The expedition was funded by the U.S. National Science Foundation (NSF); the Ministry of Education, Culture,

Sports, Science and Technology, Japan (MEXT); the European Consortium for Ocean Research Drilling; the Ministry of Science and Technology (People's Republic of China); the Korea Institute of Geoscience and Mineral Resources; the Australian Research Council and the New Zealand Institute for Geological and Nuclear Sciences; and the Ministry of Earth Sciences (India). Post-expedition analyses were funded by the NSF through the Center for Dark Energy Biosphere Investigations (C-DEBI), and by the Japan Society for the Promotion and Development (JSPS) Grants-in-Aid for Science Research (no. 26251041, 24651018, 24687004, and GR102 in NEXT Program: to F.I. and Y.M.) through the MEXT. This is C-DEBI publication XXX.

Author Contributions: S.D. and F.I. led the expedition. C.A.Z. managed the expedition project. S.D., F.I., T.F., R.P. and A.J.S. designed the study. L.J.A., N.D., T.E., H.E., T.F., B.G., R.N.H., B.W.H., J.-H.H., J.K., J.K., J.E.L., S.M., Y.M., R.W.M., R.P., T.S., F.S., C.E.S.-D., D.C.S., A.J.S., B.O.S., Y.S., M.S., L.T., G.U., Y.T.Y, G.Z., X.-H.Z. and W.Z. collected and analysed samples and data. J.S. analysed data. S.D. wrote the manuscript with significant input from F.I., T.F., J.K., R.W.M., Y.M., R.P., J.S. and A.J.S.

Author Information: All data are deposited in the IODP database and archived on-line in the IODP Expedition 329 Proceedings. Reprints and permission information are available at www.nature.com/reprints. We report no competing financial interests. Correspondence and requests for materials should be addressed to S.D. (dhondt@mail.uri.edu).

288 **Figure Legends**

289 Fig 1. Site locations and time-averaged seasurface chlorophyll-a concentrations [Global
290 SeaWiFS Chlorophyll (mean of September 1997 - December 2004)]. Colored dots mark
291 Expedition 329 site locations: U1365 (orange), U1368 (light blue), U1367 (pink), U1368
292 (green), U1369 (red)), U1370 (dark blue), and U1371 (black). Colored lines mark site
293 paleopositions with tiny dots marking site locations at 20-myr increments. Sites U1365-
294 U1370 are located within the SPG oligotrophic region and U1371 is located south of the
295 SPG oligotrophic region. White dots mark drill-sites where life in deep subseafloor
296 sediment has previously been examined.

297 Fig 2. Sedimentary profiles of cell abundance and chemical concentrations[7], keyed to site
298 location colors in Fig 1: (A) cell concentration (logarithmic scales), (B) dissolved O_2,
299 (C) dissolved NO_3^-, (D) dissolved PO_4^-, (E) dissolved inorganic carbon, (F) total organic
300 carbon. Profiles span the sediment column, from seafloor to basement. Because optode-
301 based O_2 measurements are less noisy than electrode-based measurements, the O_2
302 profiles in (A) are limited to optode data except where sedimentary fabric prevented
303 optode deployment (the lowermost portion of U1367, as well as most of U1368 and
304 U1371). Vertical line in (B) marks the minimum quantification limit (MQL). Open
305 circles in (B) mark data below the MQL.

306 Fig. 3. Net O_2 reaction rates calculated from O_2 optode data at SPG Sites U1365, U1366, U1367,
307 U1369 and U1370 (SI). Vertical dark blue lines represent mean net O_2 reduction rates,
308 light blue boxes represent the first standard deviation of the mean reaction rate, and
309 vertical lines of open dots with blue margins (ooo) mark intervals where the net O_2
310 reduction rate appears to be negative, but is indistinguishable from zero (SI). The net

311 reaction rate is also statistically indistinguishable from zero at sites and depths where the
312 O_2 reduction rate is positive and the light blue boxes intersect the left side of the panel (at
313 these depths the first standard deviation of the rate overlaps with zero). Dissolved O_2 is
314 present throughout the sediment column at all six SPG sites. We did not calculate
315 reaction rates for intervals that lack optode data (the lowermost sediment of U1367 and
316 all of U1368) and intervals disturbed by drilling (cross-hatched intervals). Basaltic
317 basement is marked by dark gray intervals.
318 Fig 4. Regions where we predict dissolved O_2 and aerobic activity to persist from seafloor to
319 igneous basement, based on mean sediment accumulation rates and mean sediment
320 thicknesses (**SI**). Red dots indicate coring sites where dissolved O_2 diffusively penetrates
321 the entire sediment column (up to 75 mbsf)[5, 7, 20]. At these sites, sediment thickness was
322 determined by drilling or piston-coring the entire sediment column. Black dots indicate
323 sites where dissolved O_2 disappears in cm to meters below the seafloor[6, 12]. Yellow dots
324 indicate sites where dissolved O_2 penetrates more than 7 to 34 mbsf and may penetrate to
325 basement but O_2 content is not fully characterized throughout the entire sediment
326 column[5, 6, 8, 20]. The dark blue area represents the minimum area over which dissolved O_2
327 permeates the entire sediment sequence and the upper basement; it is defined by
328 combinations of mean sediment thicknesses from standard global maps[33, 34] (averaged
329 over five-minute grids) and mean sediment accumulation rates comparable to the single-
330 site sediment thicknesses and sedimentation rates where O_2 is known from direct
331 measurements to penetrate the entire sediment sequence. Some sites where O_2 is known
332 to penetrate the entire sediment column are outside this region; this discrepancy results
333 from regionally interpolated estimates of mean sediment thickness[33, 34] being greater than

the sites' local sediment thicknesses determined by drilling to basement. The light blue area represents the maximum area over which dissolved O_2 permeates the entire sediment sequence from the overlying seafloor; it is defined by combinations where (i) dissolved chemical data indicate that O_2 may penetrate the entire column but chemical data resolution is too low to be certain or (ii) O_2 penetrates the entire sediment column at individual sites, but the regionally interpolated estimate of mean sediment thickness is greater than direct measurements of sediment thickness at the drilled sites. Dissolved O_2 may be present in the igneous basement over an even greater area, due to seawater advection through the basement.

344 Fig 1.

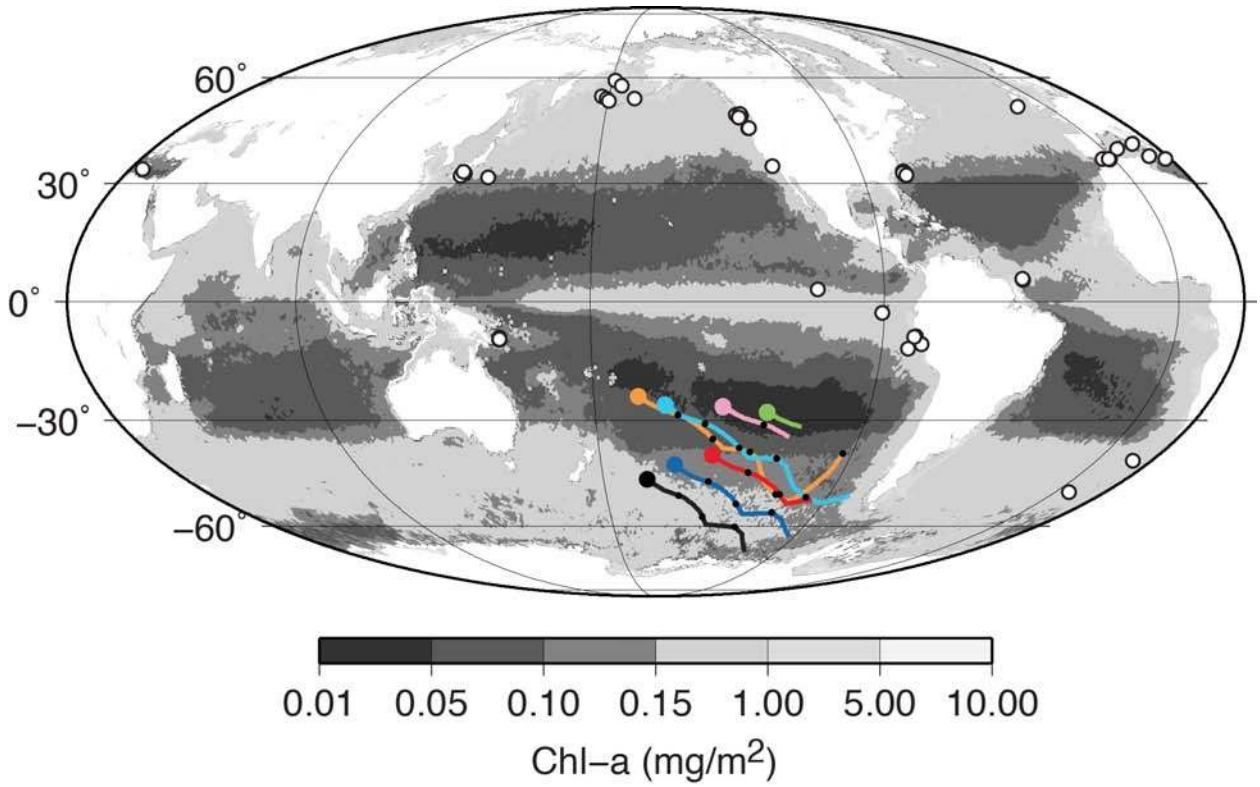

345

346

347 Fig 2.

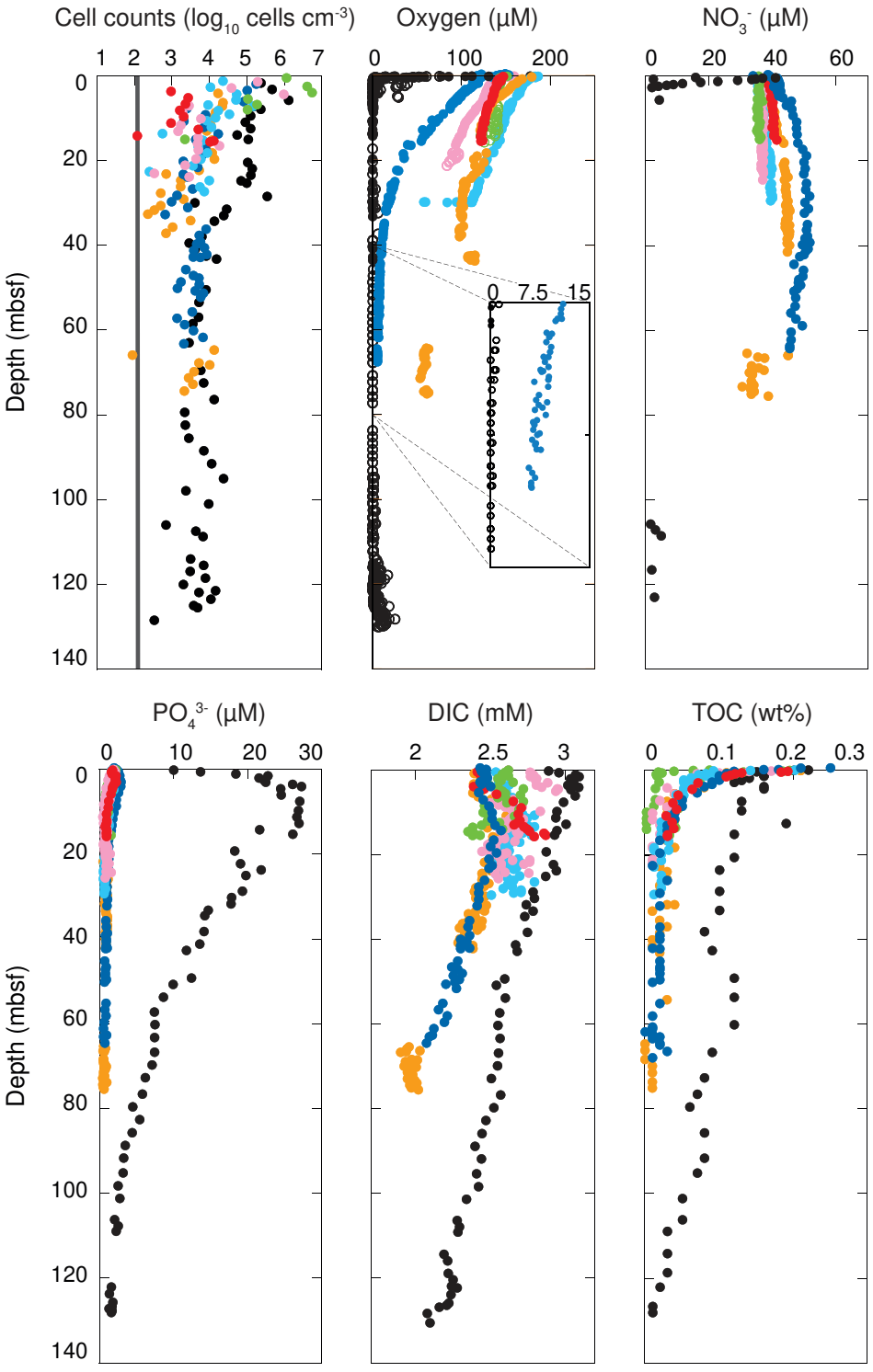

348

349

350

351 Fig 3.

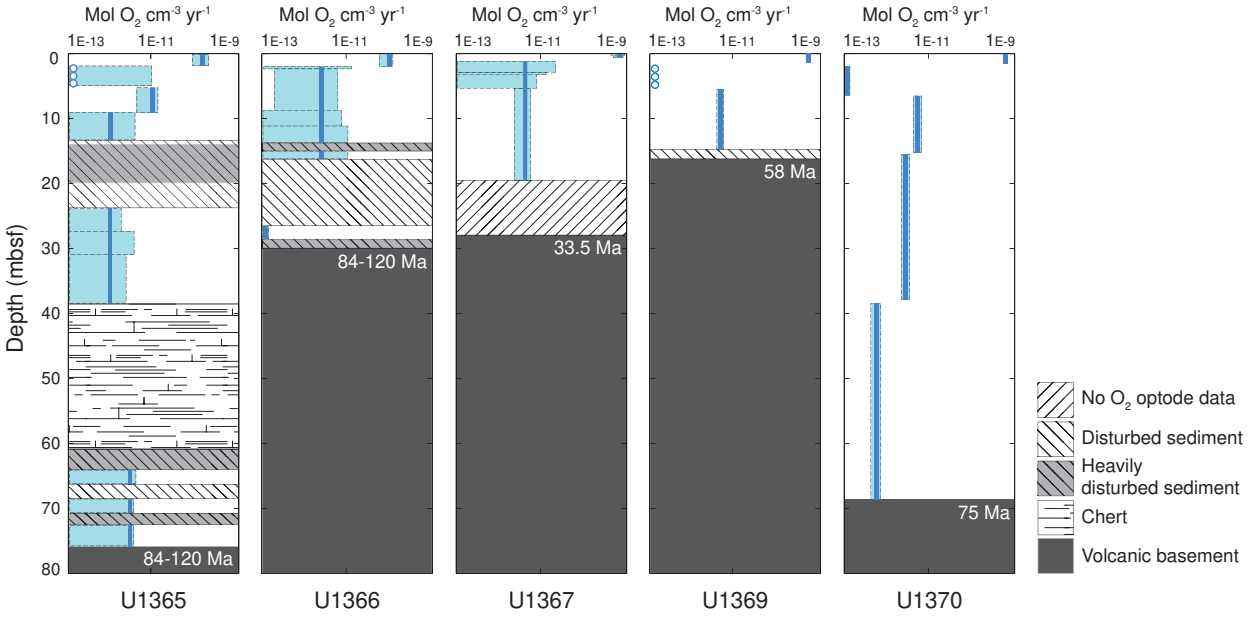

352

353

354 Fig 4.

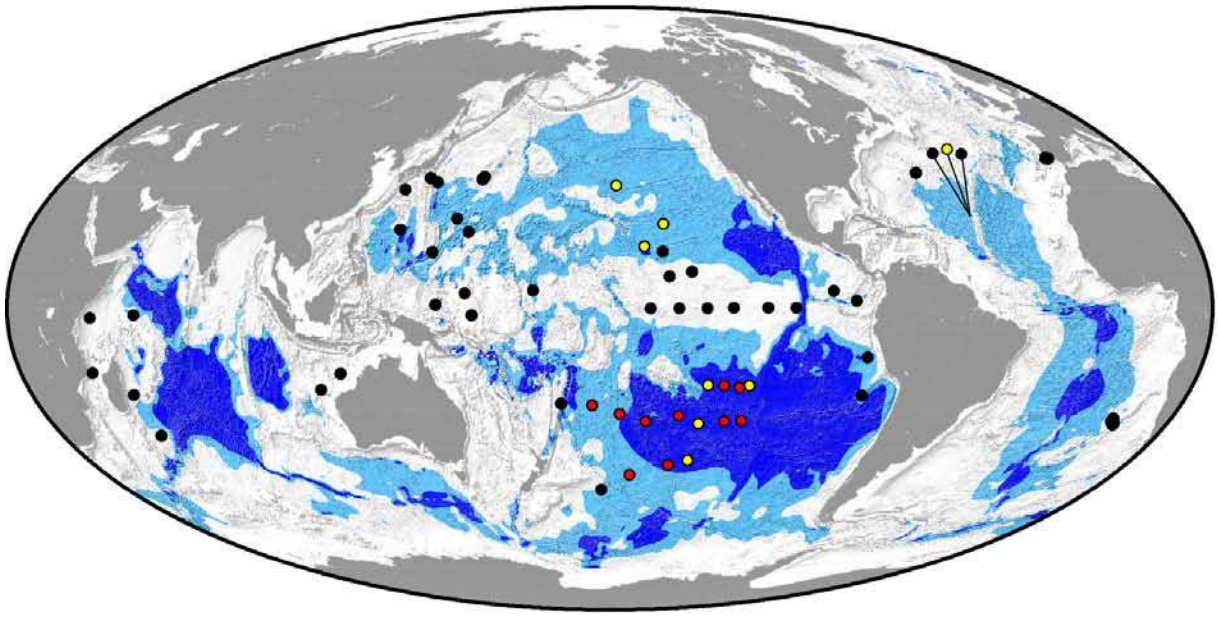

355

Supplementary Information

Chemical, physical and geological data

All Expedition 329 chemical, physical and geological data and their measurement protocols are described in reference 1. We present site details and summary results in Table 1. All samples were taken by piston coring in advance of the drill bit[1].

Cell enumeration procedures

We provide the cell-count data for this manuscript in Table 2. These are not the shipboard data in reference 1; the minimum quantification limit (MQL) for the shipboard cell counts (~10^3 cells/cm^3)[1] was too high to conclusively test the presence or absence of microbial cells in the deepest, oldest sediment of our sites. Consequently, we greatly refined the cell-counting protocols and undertook new counts for this manuscript after the expedition.

For cell enumeration, we routinely took 2-cm^3 samples from the center of cut core ends using a 3-cm^3 syringe. Each 2-cm^3 sediment plug was extruded into a sterile 15-ml centrifuge tube containing 8 ml of 2.5% (w/v) NaCl solution with 2 % (v/v) formalin as a fixative, and then thoroughly shaken to form a homogenous suspension. We performed cell counts by a fluorescence color-based cell enumeration technique using SYBR Green I fluorescent dye[2]. To evaluate low-density populations (below 10^4 cells cm^{-3}), we detached cells from sediment by using a multi-layer density gradient technique[3]. For

22 blank samples, we replaced the sediment slurry with sterile-filtered TE Buffer. We then
23 counted cell numbers by either manual or computer-based microscopic observations[2,4].
24 We defined the MQL as the mean of the blank counts plus three times their standard
25 deviation. As shown in manuscript Fig 2, the MQL for these counts is 130 cells/cm^3. We
26 carried out all filter preparation steps, including sonication of sediment and SYBR Green
27 I staining, in an ultra-clean bench placed in a HEPA-filtered clean booth at the Kochi
28 Institute for Core Sample Research, JAMSTEC.
29 We confirmed the presence of dissolved O_2 throughout the sediment column at all six
30 SPG sites by independently undertaking parallel O_2 measurements for each site using
31 fiber-optic O_2 microsensors (optodes)[5] and amperometric Clark-type O_2 sensors
32 (microelectrodes)[6]. For consistency, we used optode data for all O_2 calculations and
33 illustration, except for Sites U1368 and U1371, where optode data are limited to small
34 fractions of the sediment column; at those sites, electrode-based measurements are used
35 for illustration.
36
37 **Calculation of O_2 exposure times**
38 We calculated O_2 exposure times[7] by dividing O_2 penetration depth by sediment age
39 at the depth of O_2 penetration. For Sites U1365 to U1370, O_2 penetration depth equals
40 total sediment thickness and sediment age at the depth of O_2 penetration equals basement
41 age[1]. For Site U1371, we used mean sediment accumulation rate calculated from
42 sediment thickness and basement age to estimate sediment age at depth of O_2 penetration.
43
44 **Comparison of dissolved O_2 to dissolved NO_3^-**

Because O_2 measurements and NO_3^- measurements were made at different sediment depths and (often) in different holes, we interpolated O_2 concentrations for comparison to NO_3^- in SI Fig 1. Because the diffusion coefficient of dissolved O_2 is about 10% higher than that of NO_3^- at *in situ* temperatures[8], O_2 diffuses into the sediment slightly faster than NO_3^- diffuses out. This difference is consistent with the slight excess of NO_3^- relative to the Redfield O_2/NO_3^- respiration ratio in at the sites with greatest sediment thickness (U1365 and U1370). To account for the slight difference in diffusion coefficients of O_2 and NO_3^-, the relationship of O_2 and NO_3^- profiles to the Redfield ratio in subseafloor SPG sediment has been quantitatively tested by use of a diffusion-reaction model for the O_2 and NO_3^- data of Site U1370[9]; this test demonstrated that the best-fit $NO_3^-/-O_2$ respiration ratio is indistinguishable from the Redfield ratio throughout the sediment column.

Reaction rate calculations

We quantified vertical distributions of O_2 reaction (aerobic respiration) rates (Table 3) using the MatLab program and numerical procedures of reference 10, with dissolved O_2 concentrations, physical properties (*in situ* temperature, porosity, formation factor) and sediment burial rates from reference 1. For our calculations, we assumed fluid advection rates to be below detection. We derived our diffusion coefficients from *in situ* temperature data[1] and diffusion coefficients of O_2 in seawater at standard temperatures[8].

The algorithm for calculating reaction rates uses iterative numerical procedures to identify the maximum number of depth intervals with statistically different reaction rates at a prescribed significance level ($\alpha = 0.05$). It explicitly accounts for downhole variation

68 in physical properties and measurement spacing.

69 A key variable in this approach is the user-defined minimum number of data points
70 required to define a reaction zone. We used a minimum of either 5 data points (for Sites
71 U1365, U1367, U1369, U1370)) or 7 data points (for Site U1366) to define the minimum
72 reaction zones for our calculations after testing a range of values from 3-21 data points.
73 Our selection of these minimum reaction zones was based on the fit of an algorithm-
74 derived best-fit line to the actual O_2 measurements and the complexity or variability of
75 the defined reaction rate zones. For example, reaction zones defined by fewer than 5
76 points exhibited nice fits to the actual O_2 data, but the resulting reactions rates were very
77 erratic and unrealistic as the values often alternated rapidly between positive and negative
78 values. This erratic character resulted from rapid changes in slope of the best-fit line used
79 to derive reaction rates. For reaction zones defined by more than 7 points, the best-fit line
80 departed significantly from the actual O_2 measurements, and the reaction zones are
81 typically too broad and underestimated the characteristic reaction rate. Our selection of
82 the 5- or 7-point minimum reaction zone iteration depended on which number of points
83 per minimum zone yielded a lower uncertainty.

84 We used a Monte Carlo technique to estimate uncertainties in the calculated reaction
85 rates[10]. The key variables for the uncertainty estimate are the precision of the O_2
86 measurement and the number of reaction rate iterations. For our results, we used a 1%
87 measurement precision with 50 iterations.

88 At Sites U1365, U1369 and U1370, the program calculated brief intervals of net O_2
89 production for the second reaction zone below the seafloor. These results are essentially
90 indistinguishable from zero (see Table 3 and manuscript Fig 3) and disappear if we

calculate the mean rates over longer data intervals. Their cause is unclear, but their consistent occurrence in the second reaction interval at each site suggests that they may be an artifact of the rapid change in O_2 gradient at this depth and the very small number of data points in this reaction subzone (five).

We calculated per-cell respiration rates from these reaction rates and the cell counts in manuscript Fig 2a. These rates were converted to electron transport rates assuming transfer of 4 electrons per O_2 molecule reduced. We calculated per-cell respiration rates for equatorial Pacific ODP Site 1226 using sulfate reduction rates from reference 10, cell counts from reference 11, and assuming transfer of 8 electrons via reduction of each sulfate ion.

Predicting the global distribution of O_2 and aerobic communities from seafloor to basement

To map where oxygen may be present in the sediment from seafloor to basement, we examined the relationship between O_2 penetration to basement and several relevant variables for which there are globally extrapolated maps; these variables included estimates of mean annual seasurface chlorophyll content[12], particulate organic carbon flux at 2 km waterdepth[13], seafloor carbon deposition flux[14], organic carbon burial rate[15, 16], seafloor oxygen flux[15, 16], oxygen-equivalent carbon flux[16], sediment thickness[17, 18], and mean sedimentation rate (calculated as described below). Global extrapolations of seafloor carbon deposition flux, seafloor oxygen flux and sedimentation rate are generally correlated because seafloor carbon deposition flux and seafloor oxygen flux are typically calculated from estimates of sedimentation rate[e.g., 15, 16].

Of these variables, we found the combination of mean sediment accumulation rates and sediment thickness best explained the distribution of sites where dissolved O_2 does or does not penetrate from seafloor to basement. Consequently, we used sediment thickness and mean sediment accumulation rates to create a map that predicts where oxygen is likely to be present throughout the entire sediment column. We created the global sediment accumulation rate map by merging sediment thickness grids[17, 18] and dividing by the basement age grid[19]. For these maps, we resampled the original grids[17-19] at a 5-minute grid interval. We used Generic Mapping Tools software[20] for grid manipulations and calculations.

To define combinations of sediment thickness and sediment accumulation rate for regions with oxic sediment to basement, we used dissolved O_2 measurements[1, 21-23] or measurements of dissolved NO_3^- concentrations that approximate or exceed local bottom-water values[24]. At sites where dissolved O_2 measurements approach zero[23], we detrended the data, discarded measurements that lie outside the second standard deviation of the data profile and then determined if zero fell within the second standard deviation of the remaining measurements. To define combinations of sediment thickness and sediment accumulation rate for regions with anoxic sediment at depth, we used profiles of dissolved O_2, NO_3^-, dissolved manganese, dissolved iron, dissolved SO_4^{2-} and dissolved CH_4 from Deep Sea Drilling Project, Ocean Drilling Program and Integrated Ocean Drilling Program sites[25] and profiles of dissolved O_2 from deep piston coring sites[21, 22]. We examined dissolved chemical profiles from 401 open-ocean DSDP, ODP and IODP drill sites and 24 long-coring sites that geographically bound the regions of possible O_2 penetration to basement (425 total sites). To previent our results from being affected by

small numbers of bad measurements at individual sites, we limited this analysis to the 149 sites (of the 425) that exhibit smoothly varying concentration profiles for measurements of one or more of these dissolved chemicals. At eight sites, we used dissolved manganese as evidence of O_2 absence, following the standard assumptions that (i) manganese is not reduced in oxic environments[26, 8] and (ii) dissolved manganese is predominantly reduced [Mn(II) and $MnCl^+$ [27] or ligand-stabilized Mn(III)[28]]. However, recent studies have recorded dissolved manganese concentrations of a few micromolar in subseafloor sediment with abundant dissolved O_2 in the South Pacific Gyre[1] and the North Pacific Gyre (R.W. Murray, pers. comm. 8/14); whether these concentrations are sampling artifacts or (meta)stable concentrations of dissolved manganese in strongly oxic sediment remains to be determined.

Assessment of influence on subducting sediment

To assess effects of O_2 penetration depth on the chemistry of subducting sediment, we examined published records of sediment composition at DSDP/ODP/IODP sites seaward of subduction zones. In some regions, sediment sequences that we infer to be fully penetrated by O_2 directly enter a subduction zone (e.g., the Tonga Trench and the central and southern portions of the Peru-Chile Trench) (see manuscript Fig 4). In other regions, sedimentation rate and sediment thickness increase as the trench is approached. Despite anoxia in the upper sediment column of the latter regions, a great deal of oxidized material is present deeper in the sediment. For example, porewater chemical profiles indicate that manganese reduction is dominant in the upper sedimentary column of DSDP Site Sites 1149 and 1231, which respectively approach the Izu-Bonin Trench and the

160 northern Peru-Chile Trench[29, 11]. In such sequences, dissolved O_2 is not present in the
161 upper sediment column at the time of subduction, but oxidized iron and oxidized
162 manganese may remain abundant in solid phases at greater depth (e.g., DSDP Sites 303,
163 426, 578 and 581)[30-32] and dissolved O_2 and NO_3^- may be present in the deepest sediment
164 and the upper basement[11].
165
166 **References**

167 1 D'Hondt, S., Inagaki, F., Alvarez Zarikian, C.A., & the Expedition 329 Scientists,
168 *Proc. IODP* **329**: Tokyo (Integrated Ocean Drilling Program Management
169 International, Inc.) (2011).
170 2 Morono, Y., Terada, T., Masui, N. & Inagaki, F. Discriminative detection and
171 enumeration of microbial life in marine subsurface sediments. *ISME Journal* **3**,
172 503-511 (2009).
173 3. Morono, Y., T. Terada, J. Kallmeyer and F. Inagaki, An improved cell separation
174 technique for marine subsurface sediments: applications for high-throughput
175 analysis using flow cytometry and cell sorting, *Environ. Microbiol*. **15,** 2841-2849
176 (2013).
177 4 Morono, Y. & Inagaki, F. Automatic Slide-Loarder Fluorescence Microscope for
178 Discriminative Enumeration of Subseafloor Life. *Scientific Drilling* **9**, 32-36
179 (2010).
180 5 Fischer, J. P., Ferdelman, T.G., D'Hondt, S., Røy, H. & Wenzhöfer, F. Oxygen
181 penetration deep into the sediment of the South Pacific gyre. *Biogeosciences* **6**,
182 1467-1478 (2009).

183 [6] Revsbech, N.P. An oxygen microsensor with a guard cathode. *Limnol. Oceanogr.*
184 **34**, 474-478 (1989).
185 [7] Hartnett, H.E., R.G. Keil, J.I. Hedges and A.H. Devol, Influence of oxygen
186 exposure time on the preservation of organic carbon in continental margin
187 sediments, *Nature* **391** 572-574 (1998).
188 [8] Schulz, H.D. in *Marine Geochemistry*, H. D. Schulz, M. Zabel, Eds. (Springer-
189 Verlag, Heidelberg, New York, 2000), 85–128.
190 [9] Huang, Y., "The NO_3^-/-O_2 respiration ratio of the deep sedimentary biosphere in
191 the Pacific gyres" (2014). *Dissertations and Master's Theses (Campus Access).*
192 Paper AAI1555654. http://digitalcommons.uri.edu/dissertations/AAI1555654.
193 [10] Wang, G., A.J. Spivack, S. Rutherford, U. Manor and S. D'Hondt, Quantification
194 of co-occurring reaction rates in deep subseafloor sediments, *Geochim.*
195 *Cosmochim. Ac.* 72, 3479-3488 (2008).
196 [11] D'Hondt, S., and 34 others, Distributions of microbial activities in deep
197 subseafloor sediments, *Science* 306, 2216-2221.
198 [12] Global SeaWiFS Chlorophyll (mean of September 1997 - December 2004
199 [13] Henson, S.A., R. Sanders and E Madsen, Global patterns in efficiency of
200 particulate organic carbon export and transfer to the deep ocean, Global
201 Biogeochemical Cycles 26, GB1028 (2012).
202 [14] Dunne, J. P., J.L. Sarmiento, and A. Gnanadesikan, A synthesis of global particle
203 export from the surface ocean and cycling through the ocean interior and on the
204 seafloor, *Global Biogeochem. Cycles* **20** (2007).

205 [15] Jahnke, R.A. and G.A. Jackson, The spatial distribution of sea floor oxygen
206 consumption in the Atlantic and Pacific Oceans, in Rowe, G.T., and Parient, V.,
207 eds., Deep-Sea Food Chains and the Global Carbon Cycle, p. 295-307 (1992).
208 [16] Jahnke, R. A. The global ocean flux of particulate organic carbon: areal
209 distribution and magnitude. *Global Biogeochem. Cycles* **10**, 71-88 (1996).
210 [17] Divins D.L. NGDC Total Sediment Thickness of the World's Oceans & Marginal
211 Seas (NOAA) (2008).
212 [18] Laske, G. and G.A. Masters, global digital map of sediment thickness. *EOS*
213 *Trans. AGU* 78, F483 (1997).
214 [19] Müller R. D., Sdrolias M., Gaina C., & Roest W. R. Age, spreading rates, and
215 spreading asymmetry of the world's ocean crust. *Geochem. Geophys. Geosy.* **9**
216 (2008).
217 [20] Wessel P. & Smith W.H.F. New, inproved version of the Generic Mapping Tools
218 released. *EOS Trans. AGU.* 79, 579 (1998).
219 [21] D'Hondt, S. *et al.* Subseafloor sedimentary life in the South Pacific Gyre. *Proc.*
220 *Nat. Acad. Sci. U.S.A.* **106**, 11651-11656 (2009).
221 [22] Røy, H., J. Kallmeyer, R.R. Adhikari, R. Pockalny, B.B Jørgensen and S.
222 D'Hondt, Aerobic microbial respiration in 86-million-year-old deep-sea red clay,
223 *Science* 336 (6083), 922-925 (2012). Erratum (figure correction) in *Science* 336
224 (6088), 1506 (2012).
225 [23] Orcutt, B.N., et al., Oxygen consumption rates in subseafloor basaltic crust
226 derived from a reaction transport model, *Nat. Commum.* **4**, 2539 (2013).

[24] Gieskes, J.M. and J. Boulegue, Interstitial Water Studies, Leg-92, *Init. Rep. DSDP* **92**, 423-429 (1986).

[25] DSDP/ODP/IODP Core database. College Station, TX: International Ocean Discovery Program. <http://iodp.tamu.edu/database/index.html>

[26] Froelich, P. N., Klinkhammer, G. P., Bender, M. L., Luedtke, N. A., Heath, G. R., Cullen, D., Dauphin, P., Hammond, D., Hartman, B., & Maynard. V. Early oxidation of organic matter in pelagic sediments of the eastern equatorial Atlantic: suboxic diagenesis, *Geochim. Cosmochim. Ac.* **43**, 1075-1090 (1979).

[27] Bruland, K. Trace elements in seawater, in *Chemical Oceanography*, 2nd Edition, Vol. **8** (ed. Riley, J. P., & Chester, R.), Academic, London, 147-220 (1983).

[28] Madison, A. S., Tebo, B. M., Mucci, A., Sundby, B. & Luther, G. W. III, Abundant porewater Mn(III) is a major component of the sedimentary redox system, *Science* **341**, 875-878 (2013).

[29] Shipboard Scientific Party, 2000. Site 1149. *In* Plank, T., Ludden, J.N., Escutia, C., et al., *Proc. ODP, Init. Repts.,* 185 [Online]. Available from World Wide Web: <http://www-odp.tamu.edu/publications/185_IR/chap_03/chap_03.htm>.

[30] Larson, R.L., and 9 others, Site 303: Japanese Magnetic Lineations, in R.L. Larson, R. Moberly et al., *Initial Reports DSDP* **32**, Washington D.C. (U.S. Government Printing Office) (1975).

[31] Shipboard Scientific Party, with P.S. Doyle, 5. Site 578, in G.R. Heath, L.H. Burckle et al., Initial Reports DSDP 86, Washington D.C. (U.S. Government Printing Office) (1985).

[32] Heath, G.R., R.B. Kovar and C. Lopez, Geochemistry of Sediments at Sites 579, 580, and 581, Deep Sea Drilling Project Leg 86, Western North Pacific, in G.R. Heath, L.H. Burckle et al., Initial Reports DSDP 86, Washington D.C. (U.S. Government Printing Office) (1985).

[33] Anderson, L.A. and J.L. Sarmiento, Global ocean phosphate and oxygen simulations. *Glob. Biogeochem. Cy.* **9**, 621-636 (1995).

Table 1. Site properties[1] and depth-integrated O_2 reduction rates below 1.5 mbsf. n.d. = not determinable (no optode data). n.a. = not applicable (O_2 does not penetrate to 1.5 mbsf at U1371).

Site	Latitude	Longitude	Water depth (m)	Seasurface chl-a concentration (mg Chl-a/m^3)	Total sediment thickness (m)	O_2 exposure time (Ma)	O_2 consumption in sediment >1.5 mbsf (mol/cm^2/yr)
Within gyre							
U1365	-23°51'	-165°39’	5695	0.057	75	84 - 120	-2.20E-08
U1366	-26°03'	-156°54’	5127	0.054	30	84 - 120	-6.28E-09
U1367	-26°29'	-137°56’	4289	0.035	27	33.5	-2.03E-09
U1368	-27°55'	-123°10’	3740	0.030	16	13.5	n.d.
U1369	-39°19'	-139°48’	5277	0.110	16	58	-3.24E-09
U1370	-41°51'	-153°06’	5075	0.138	68	75	-1.77E-08
Outside gyre							
U1371	-45°58'	-163°11’	5305	0.199	131	0.035	n.a.

263 **Table 2.** Post-expedition cell counts for Expedition 329 sites. The cell counts shown in
264 manuscript Fig 2a and used for our per-cell reaction rate calculations (Table 3)
265 were limited to counts from sedimentary intervals described by shipboard
266 scientists as characterized by no visible sediment disturbance or only slight
267 disturbance[1]. Counts from sediment described by shipboard scientists[1] as heavily
268 disturbed, moderately disturbed or affected by flow-in were excluded from
269 manuscript Fig 2a and our per-cell calculations. Define disturbance notes of
270 fourth column. The extent of sediment disturbance at each sampling depth is
271 identified in the Disturbance intensity column as follows: H (heavily disturbed),
272 M (moderately disturbed, S (slightly disturbed), F (flow-in). Intervals free of
273 visible disturbance are left blank in the Disturbance intensity column.
274

Site	Hole	core	section	cm interval	Depth (mbsf)	Cell abundance (cells / cm^3)	Disturbance intensity
U1365	B	1	1	40-50	0.5	5.14×10^5	H
U1365	B	1	2	40-50	2.0	5.29×10^4	M
U1365	B	1	3	40-50	3.5	3.02×10^4	M
U1365	B	2	1	75-85	4.9	1.69×10^4	
U1365	B	2	2	140-150	7.1	2.27×10^4	
U1365	B	2	3	75-85	7.9	2.19×10^4	
U1365	B	2	4	75-85	9.4	1.44×10^4	
U1365	B	2	5	75-85	10.9	1.00×10^4	
U1365	B	2	6	75-85	12.4	1.06×10^4	
U1365	B	2	7	58-68	13.7	8.41×10^3	
U1365	B	3	1	75-85	14.4	1.31×10^4	S
U1365	B	3	2	75-85	15.9	1.18×10^4	
U1365	B	3	3	75-85	17.4	8.00×10^3	
U1365	B	3	4	75-85	18.9	1.17×10^4	
U1365	B	3	5	75-85	20.4	1.33×10^4	
U1365	B	3	6	75-85	21.9	4.43×10^3	
U1365	B	3	7	40-50	23.1	5.22×10^3	

U1365	B	4	1	75-85	23.9	6.91×10^{2}	
U1365	B	4	2	75-85	25.4	1.71×10^{3}	
U1365	B	4	3	75-85	26.9	1.69×10^{3}	
U1365	B	4	4	75-85	28.4	4.96×10^{2}	
U1365	B	4	5	75-85	29.9	2.04×10^{3}	
U1365	B	4	6	75-85	31.4	4.96×10^{2}	
U1365	B	4	7	25-30	32.4	3.34×10^{2}	
U1365	B	5	1	75-85	33.4	2.26×10^{2}	
U1365	B	5	2	75-85	34.9	3.08×10^{3}	
U1365	B	5	3	75-85	36.4	1.03×10^{3}	
U1365	B	5	4	75-85	37.9	6.84×10^{2}	
U1365	B	5	5	65-75	39.3	1.43×10^{3}	S
U1365	B	5	6	75-85	40.9	6.64×10^{2}	H
U1365	B	5	7	63-73	42.3	6.67×10^{2}	H
U1365	B	8	2	40-50	65.5	1.33×10^{4}	
U1365	B	8	3	55-65	66.6	8.70×10^{1}	
U1365	B	9	1	140-149	68.4	5.17×10^{3}	
U1365	B	9	2	40-50	69.0	1.01×10^{4}	
U1365	B	9	3	40-50	70.5	3.86×10^{2}	
U1365	B	9	4	40-50	72.0	2.76×10^{3}	
U1365	B	9	5	40-50	73.5	3.60×10^{3}	
U1365	B	9	6	50-60	74.7	4.99×10^{3}	
U1365	B	9	6	50-60	75.1	2.10×10^{3}	
U1365	B	9	6	50-60	75.6	4.55×10^{3}	

U1366	D	1	2	40-50	2.0	2.27×10^{4}	
U1366	D	1	3	40-50	3.5	1.05×10^{4}	
U1366	D	1	4	50-60	5.1	5.23×10^{4}	
U1366	D	1	5	40-50	6.5	5.10×10^{4}	
U1366	D	1	6	40-50	8.0	1.43×10^{5}	
U1366	D	1	7	20-30	9.0	1.71×10^{4}	
U1366	D	2	1	40-50	9.9	3.36×10^{4}	
U1366	D	2	2	40-50	11.4	8.32×10^{3}	
U1366	D	2	3	40-50	12.9	1.11×10^{4}	
U1366	D	2	4	40-50	14.4	5.56×10^{2}	
U1366	D	2	6	40-50	17.2	2.75×10^{3}	
U1366	F	2	2	60-70	7.7	9.15×10^{2}	
U1366	F	2	4	60-70	10.7	1.44×10^{4}	
U1366	F	3	1	40-50	14.5	5.44×10^{3}	H
U1366	F	3	2	40-50	16.0	6.67×10^{3}	
U1366	F	3	3	40-50	17.5	4.99×10^{3}	
U1366	F	3	4	40-50	19.0	8.74×10^{3}	
U1366	F	3	5	40-50	20.5	5.75×10^{3}	
U1366	F	3	6	40-50	22.0	3.55×10^{3}	
U1366	F	3	7	30-41	23.4	2.48×10^{2}	

U1366	F	4	1	40-50	24.0	5.61×10^{3}	H
U1366	F	4	2	40-50	25.3	5.67×10^{3}	
U1366	F	4	2	40-50	25.5	9.81×10^{3}	
U1366	F	4	3	40-50	27.0	5.49×10^{3}	
U1366	F	4	4	0-10	28.1	7.18×10^{3}	
U1366	F	4	5	50-59	29.5	8.84×10^{3}	H
U1366	F	4	5	40-50	30.1	7.47×10^{5}	H
U1367	C	1	1	10-20	0.2	2.31×10^{5}	S
U1367	C	1	2	60-70	2.2	1.91×10^{5}	
U1367	C	1	3	60-70	3.7	3.84×10^{4}	
U1367	C	1	4	60-70	5.2	9.56×10^{5}	
U1367	C	1	5	60-70	6.7	1.06×10^{3}	S
U1367	C	2	1	60-70	7.9	2.82×10^{3}	
U1367	C	2	2	60-70	9.4	1.89×10^{3}	
U1367	C	2	3	60-70	10.9	5.90×10^{3}	
U1367	C	2	4	60-70	12.4	1.70×10^{3}	
U1367	C	2	5	60-70	13.9	1.43×10^{3}	
U1367	C	2	6	60-70	15.4	4.90×10^{3}	
U1367	C	2	7	50-60	16.8	4.79×10^{3}	
U1367	C	3	1	50-60	17.3	1.82×10^{4}	
U1367	C	3	2	0-5	18.2	5.00×10^{3}	
U1367	C	3	3	60-70	20.4	4.38×10^{3}	
U1367	C	3	4	60-70	21.9	2.23×10^{3}	
U1367	C	3	6	0-5	23.6	6.04×10^{3}	F
U1367	D	2	4	50-60	12.5	4.31×10^{5}	S
U1367	D	3	1	80-90	17.8	2.42×10^{4}	S
U1367	D	3	2	10-20	18.6	1.28×10^{6}	S
U1367	D	3	3	10-20	20.1	7.45×10^{4}	S
U1367	D	3	4	80-90	22.3	2.23×10^{3}	S
U1367	D	3	5	80-90	23.8	3.34×10^{2}	
U1367	D	3	6	10-20	24.6	2.85×10^{3}	
U1368	C	1	1	10-15	0.1	1.13×10^{6}	
U1368	C	1	2	60-70	2.2	4.04×10^{6}	
U1368	C	1	3	60-70	3.7	5.45×10^{6}	
U1368	C	1	4	60-70	5.2	1.05×10^{5}	
U1368	C	1	5	40-50	6.5	1.85×10^{5}	
U1368	C	1	6	10-20	7.7	1.04×10^{5}	
U1368	C	2	1	50-60	8.6	3.43×10^{3}	S
U1368	C	2	2	60-70	10.2	5.07×10^{3}	S
U1368	C	2	3	60-70	11.7	2.40×10^{3}	S
U1368	C	2	4	60-70	13.2	7.85×10^{3}	S
U1368	C	2	5	60-70	14.7	2.19×10^{3}	

U1368	C	2	6	10-20	15.6	1.31×10^{5}	H
U1369	C	1	1	15-20	0.2	4.83×10^{5}	H
U1369	C	1	2	50-60	2.1	6.18×10^{3}	H
U1369	C	1	3	50-60	3.6	9.93×10^{2}	
U1369	C	1	4	50-60	5.1	2.85×10^{3}	
U1369	C	2	1	50-60	6.6	2.41×10^{3}	
U1369	C	2	2	50-60	8.1	1.71×10^{3}	
U1369	C	2	3	50-60	9.6	2.16×10^{3}	
U1369	C	2	4	50-60	11.1	9.99×10^{2}	
U1369	C	2	5	50-60	12.6	5.34×10^{3}	
U1369	C	2	6	50-60	14.1	1.24×10^{2}	
U1369	C	2	7	45-54	15.5	1.09×10^{4}	
U1369	E	2	6	90-100	15.3	1.38×10^{4}	
U1370	E	1	1	35-42.5	0.4	9.55×10^{5}	S
U1370	E	1	2	30-40	1.9	1.88×10^{5}	
U1370	E	1	3	30-40	3.4	1.07×10^{5}	
U1370	E	1	4	147-152	6.0	8.67×10^{4}	
U1370	E	2	1	135-140	7.6	2.62×10^{3}	
U1370	E	2	2	135-140	9.1	8.31×10^{3}	
U1370	E	2	3	135-140	10.6	2.19×10^{3}	
U1370	E	2	4	125-130	12.0	7.58×10^{3}	
U1370	E	2	5	135-140	13.6	1.81×10^{4}	
U1370	E	2	6	118-123	14.9	4.53×10^{3}	
U1370	E	3	1	135-140	17.1	8.19×10^{3}	
U1370	E	3	2	135-140	18.6	6.78×10^{3}	
U1370	E	3	3	135-140	20.1	2.11×10^{3}	
U1370	E	3	4	125-130	21.5	5.11×10^{3}	
U1370	E	3	5	135-140	23.1	2.12×10^{3}	
U1370	E	3	6	53-58	23.8	2.76×10^{3}	
U1370	E	4	1	135-140	26.6	3.79×10^{3}	
U1370	E	4	2	135-140	28.1	1.43×10^{3}	
U1370	E	4	3	135-140	29.6	1.03×10^{3}	
U1370	E	4	4	125-130	31.0	2.78×10^{3}	
U1370	E	4	5	135-140	32.6	6.91×10^{2}	
U1370	E	5	1	135-140	36.1	8.61×10^{3}	
U1370	E	5	2	129-134	37.5	5.67×10^{3}	
U1370	E	5	3	135-140	39.0	6.05×10^{3}	
U1370	E	5	4	125-130	40.4	7.71×10^{3}	
U1370	E	5	5	135-140	42.0	8.93×10^{3}	
U1370	E	5	6	55-60	42.7	5.97×10^{3}	
U1370	E	6	1	135-140	45.6	2.48×10^{3}	
U1370	E	6	2	124-134	47.0	3.91×10^{3}	

U1370	E	6	3	135-140	48.5	1.85×10^{3}	
U1370	E	6	4	135-140	50.0	1.47×10^{3}	
U1370	E	6	5	95-100	51.1	7.23×10^{3}	
U1370	E	8	2	135-140	58.3	2.06×10^{3}	H
U1370	E	8	3	135-140	59.8	5.08×10^{3}	F
U1370	E	8	4	125-130	61.2	7.13×10^{3}	F
U1370	E	8	5	135-140	62.8	3.74×10^{3}	F
U1370	E	9	1	135-140	63.5	6.57×10^{3}	F
U1370	E	8	6	135-140	64.3	6.57×10^{3}	F
U1370	E	9	2	135-140	65.0	4.43×10^{3}	F
U1370	F	5	3	135-140	39.6	4.87×10^{3}	
U1370	F	5	4	135-140	41.1	4.06×10^{3}	
U1370	F	5	5	135-140	42.6	3.90×10^{3}	
U1370	F	6	2	135-140	47.6	5.50×10^{3}	
U1370	F	6	3	135-140	49.1	5.68×10^{3}	
U1370	F	6	4	135-140	50.6	4.41×10^{3}	
U1370	F	6	5	135-140	52.1	6.17×10^{3}	
U1370	F	7	1	135-140	55.6	3.65×10^{3}	
U1370	F	7	2	135-140	57.1	1.45×10^{3}	
U1370	F	7	3	135-140	58.6	2.29×10^{3}	
U1370	F	7	4	125-130	60.0	3.94×10^{3}	
U1370	F	7	5	135-140	61.6	7.09×10^{3}	
U1370	F	7	6	135-140	63.1	2.19×10^{3}	

U1371	E	1	1	30-40	0.4	4.91×10^{5}	H
U1371	E	1	2	30-40	1.9	2.37×10^{5}	
U1371	E	1	3	30-40	3.4	4.65×10^{5}	
U1371	E	1	4	135-140	5.9	1.29×10^{6}	
U1371	E	1	5	135-140	7.4	1.48×10^{5}	
U1371	E	1	6	52-57	8.0	2.33×10^{5}	
U1371	E	2	1	135-140	9.6	1.25×10^{5}	
U1371	E	2	2	135-140	11.1	9.06×10^{4}	
U1371	E	2	3	135-140	12.6	1.24×10^{5}	
U1371	E	2	4	135-140	14.1	5.41×10^{4}	
U1371	E	2	5	90-95	15.1	1.07×10^{5}	
U1371	E	3	2	135-140	20.6	1.05×10^{5}	
U1371	E	3	3	125-130	22.0	1.38×10^{5}	
U1371	E	3	4	135-140	23.6	1.27×10^{5}	
U1371	E	3	5	115-120	24.9	6.93×10^{4}	
U1371	E	3	6	41-46	25.4	9.82×10^{4}	
U1371	E	4	1	135-140	28.6	3.45×10^{5}	
U1371	E	4	2	135-140	30.1	4.05×10^{3}	
U1371	E	4	3	135-140	31.6	2.85×10^{4}	
U1371	E	4	4	135-140	33.1	2.38×10^{4}	
U1371	E	4	5	115-120	34.4	1.34×10^{4}	

U1371	E	5	1	135-140	38.1	6.20×10^{3}	
U1371	E	5	2	135-140	39.6	2.85×10^{3}	
U1371	E	5	3	135-140	41.1	4.07×10^{3}	
U1371	E	5	4	135-140	42.6	8.15×10^{3}	
U1371	E	5	5	60-65	43.3	1.53×10^{4}	
U1371	E	6	3	135-140	50.6	7.95×10^{3}	H
U1371	E	6	5	135-140	53.6	5.16×10^{3}	
U1371	E	7	1	135-140	57.1	5.11×10^{3}	H
U1371	E	7	2	135-140	58.6	3.61×10^{3}	
U1371	E	7	3	125-130	60.0	5.20×10^{3}	H
U1371	E	7	5	135-140	63.1	2.84×10^{3}	
U1371	E	8	1	135-140	66.6	2.81×10^{3}	H
U1371	E	8	3	135-140	69.6	5.76×10^{3}	
U1371	E	8	5	135-140	72.6	6.91×10^{3}	
U1371	E	9	2	135-140	76.5	1.33×10^{4}	
U1371	E	9	4	135-140	79.5	2.17×10^{3}	
U1371	E	9	6	135-140	82.5	2.25×10^{3}	
U1371	E	10	1	135-140	85.6	2.79×10^{3}	
U1371	E	10	3	135-140	88.6	6.97×10^{3}	
U1371	E	10	5	135-140	91.6	1.13×10^{4}	
U1371	E	11	1	135-140	95.1	2.35×10^{4}	
U1371	E	11	3	125-130	98.0	2.32×10^{3}	
U1371	E	11	5	135-140	101.1	9.46×10^{3}	
U1371	E	12	2	135-140	106.1	6.86×10^{2}	
U1371	E	12	3	125-130	107.5	4.30×10^{3}	
U1371	E	12	4	108-118	108.8	6.66×10^{3}	
U1371	E	13	1	135-140	114.1	3.10×10^{3}	
U1371	E	13	2	135-140	115.6	6.89×10^{3}	
U1371	E	13	3	125-130	117.0	3.02×10^{3}	
U1371	E	13	4	135-140	118.6	7.68×10^{3}	
U1371	E	13	5	135-140	120.1	1.99×10^{3}	
U1371	E	13	6	135-140	121.6	1.43×10^{4}	
U1371	E	13	7	24-29	122.0	5.19×10^{3}	
U1371	E	14	1	135-140	123.6	1.08×10^{4}	
U1371	E	14	2	135-140	125.1	3.79×10^{3}	
U1371	E	14	3	30-40	125.6	4.78×10^{3}	
U1371	E	14	5	30-40	128.6	3.32×10^{2}	
U1371	E	14	6	51-56	130.2	1.57×10^{4}	F

275
276

277 **Table 3.** Vertical distribution of O_2 reaction rates (net respiration) at Expedition 329

278 sites**.**

Interval	# data points in each zone	Depth (mbsf)	Reaction rate ± 1*sigma (mol O_2/cm^3/yr)	Net respiration rate per cell ± 1*sigma (mol O_2/cell/yr)
Site U1365				
1	4	0.25 - 2.18	-8.68E-11 ± 3.68E-11	-3.06E-16 ± 3.76E-16
2	5	2.38 - 4.69	4.63E-12 ± 1.86E-11	1.97E-16 ± 7.95E-16
3	6	4.89 - 8.76	-1.52E-11± 8.49E-12	-6.83E-16 ± 3.82E-16
4	25	8.95 - 12.81	-9.28E-13 ± 6.13E-12	-9.98E-17 ± 6.60E-16
		24.95 - 27.20	-9.28E-13 ± 1.27E-12	-5.46E-16 ± 7.45E-16
		27.95 - 30.95	-9.28E-13 ± 3.84E-12	-7.33E-16 ± 3.10E-16
		31.18 - 37.95	-9.28E-13 ± 1.95E-12	-8.99E-16 ± 2.15E-16
5	13	64.45 - 65.95	-8.45E-12 ± 2.52E-12	-1.26E-15 ± 1.80E-15
		69.04 - 71.05	-8.45E-12 ± 1.96E-12	-1.52E-15 ± 1.13E-15
		74.45 - 75.05	-8.45E-12 ± 1.96E-12	-2.96E-15 ± 1.30E-15
Site U1366				
1	7	0.25 - 2.26	-6.27E-11 ± 2.22E-11	-2.77E-15 ± 1.44E-15
2	22	2.41 - 2.87	-2.67E-12 ± 1.25E-11	-8.49E-17 ± 4.04E-17
		3.03 - 8.27	-2.67E-12 ± 2.36E-12	-3.93E-17 ± 5.29E-17
		8.43 - 11.82	-2.67E-12 ± 2.88E-12	-1.45E-16 ± 1.79E-16
		11.98 - 14.29	-2.67E-12 ± 9.78E-12	-2.75E-16 ± 1.01E-16
		14.45 - 14.76	-2.67E-12 ± 9.84E-12	-8.90E-16 ± 3.44E-16
Site U1367				
1	8	0.05 - 0.5	-5.34E-10 ± 1.70E-10	-2.13E-15 ± 7.89E-16
		0.65 - 1.10	-5.34E-10 ± 1.28E-10	-2.79E-15 ± 1.71E-15
2	19	1.70 - 3.35	-1.55E-12 ± 1.73E-11	-8.11E-18 ± 3.11E-18
		3.50 - 3.80	-1.55E-12 ± 1.65E-11	-3.12E-18 ± 3.34E-18
		3.95 - 5.75	-1.55E-12 ± 5.36E-12	-3.24E-18 ± 1.27E-18
		5.90 - 18.8	-1.55E-12 ± 9.67E-13	-1.04E-17 ± 2.72E-17
Site U1369				
1	6	0.3 - 1.32	-1.72E-10 ± 6.35E-12	-3.56E-16 ± 2.49E-16
2	5	1.44 - 4.98	4.43E-12 ± 6.35E-13	1.33E-15 ± 1.06E-15
3	14	5.10 - 14.00	-3.59E-12 ± 1.51E-13	-1.69E-15 ± 1.42E-15
Site U1370				
1	15	0.05 - 1.64	-3.38E-10 ± 2.45E-12	-5.19E-16 ± 5.61E-16
2	12	1.81 - 6.23	7.64E-13 ± 7.42E-13	7.88E-18 ± 7.74E-18
3	12	6.40 - 15.22	-5.04E-12 ± 5.32E-13	-6.98E-16 ± 5.74E-16
4	13	15.40 - 37.29	-2.39E-12 ± 1.22E-13	-6.08E-16 ± 4.18E-16
5	37	37.46 - 68.00	-3.28E-13 ± 3.92E-14	-6.98E-17 ± 3.14E-17

279

Fig 1. Dissolved O_2 concentrations vs. dissolved NO_3^- concentrations at Sites U1365-U1370. Symbol colors as in manuscript Fig 1. Most data closely match the Redfield ratio [black line[33]]. Data from the two sites with thinnest sediment (youngest) basement (U1367 and U1368) fall below the Redfield line because their O_2 concentrations are primarily controlled by O_2 loss to the underlying basement. Data from below 30 mbsf at U1370 fall below Redfield at low O_2 concentrations because NO_3^- concentrations at greater depth are affected by loss to the underlying basement. These non-Redfield losses (of O_2 to the basement at U1367 and U1368, and of NO_3^- to basement at U1370) are consistent with non-heterotrophic (lithotrophic) microbial processes in the basement.

Fig 2. Regions where we predict dissolved O_2 and aerobic activity to persist from seafloor to igneous basement, based on sediment thickness and mean sediment accumulation rates. (A) Sediment accumulation rate and sediment thickness at sites where O_2 does or does not penetrate to basement. Sediment thicknesses at these sites were determined by direct measurement (drilling or piston-coring to basement). Red dots indicate sites where dissolved O_2 diffusively penetrates the entire sediment column (up to 75 mbsf)[1, 21, 24]. Black dots indicate sites where dissolved O_2 disappears in cm to meters below the seafloor[1, 11, 21-24,]. Yellow dots indicate sites where dissolved O_2 penetrates more than 7 to 34 mbsf and may penetrate to basement but O_2 content is not fully characterized throughout the entire sediment column[21, 22, 24]. (B) Global map predicted from relationships in (A), combined with mean sediment thicknesses and mean sediment accumulation rates defined by standard global maps of sediment thickness[17, 18] and seafloor

303 age[19] averaged over fine-minute grids.

304 The blue areas in 2A and 2B are defined by combinations of sediment
305 thickness and mean sediment accumulation where O_2 is known to penetrate the
306 entire sediment sequence; they represent a minimum estimate of the area over
307 which dissolved O_2 permeates the entire sediment sequence and the upper
308 basement (9% of global seafloor in 2B). The green areas are defined by
309 combinations where O_2 may penetrate the entire column but chemical data
310 resolution is too low to be certain (13% of seafloor in 2B). The orange areas mark
311 combinations of mean sediment accumulation and sediment thickness for which
312 O_2 may penetrate to basement but there are no O_2 or NO_3^- data (3% of seafloor in
313 2B). Because estimated mean sediment thicknesses in five-minute grids
314 throughout the ocean[17, 18] often differ from local sediment thicknesses determined
315 by drilling or piston-coring to basement, not all sites where O_2 penetrates to
316 basement in 2A are located in the blue areas in 2B. The combined yellow, green
317 and blue areas in both 2A and 2B are defined by the combinations of mean
318 sedimentation rates and sediment thicknesses from the standard sediment-
319 thickness maps[17, 18] that include all locations where dissolved O_2 is known to
320 locally penetrate the entire sediment column (34% of seafloor in 2B). The sum of
321 the blue, green, yellow and orange regions represents a maximum estimate of the
322 area over which dissolved O_2 permeates the entire sediment sequence from the
323 seafloor (37% of total seafloor in 2B). These collective regions broadly include all
324 areas of abyssal clay and slowly accumulating carbonate ooze in the world ocean.
325

326 Fig 1.

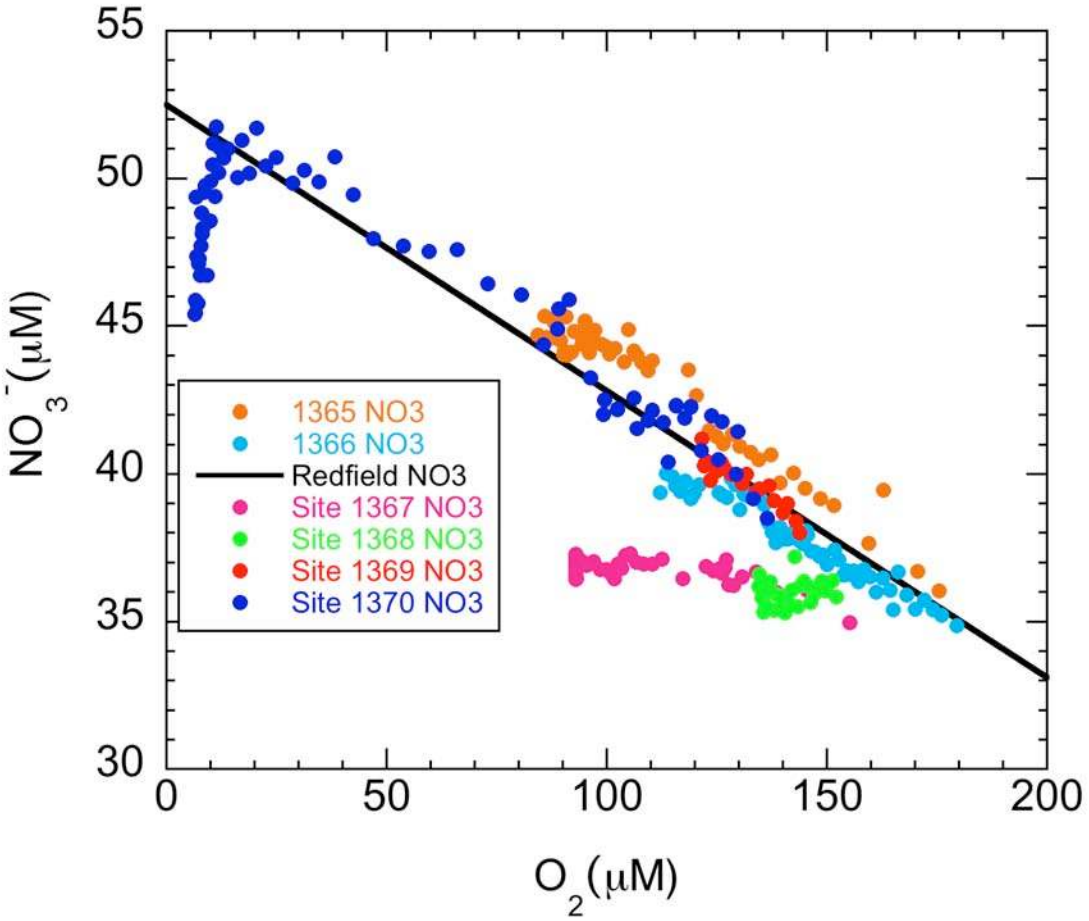

327

328

329 Fig 2A.

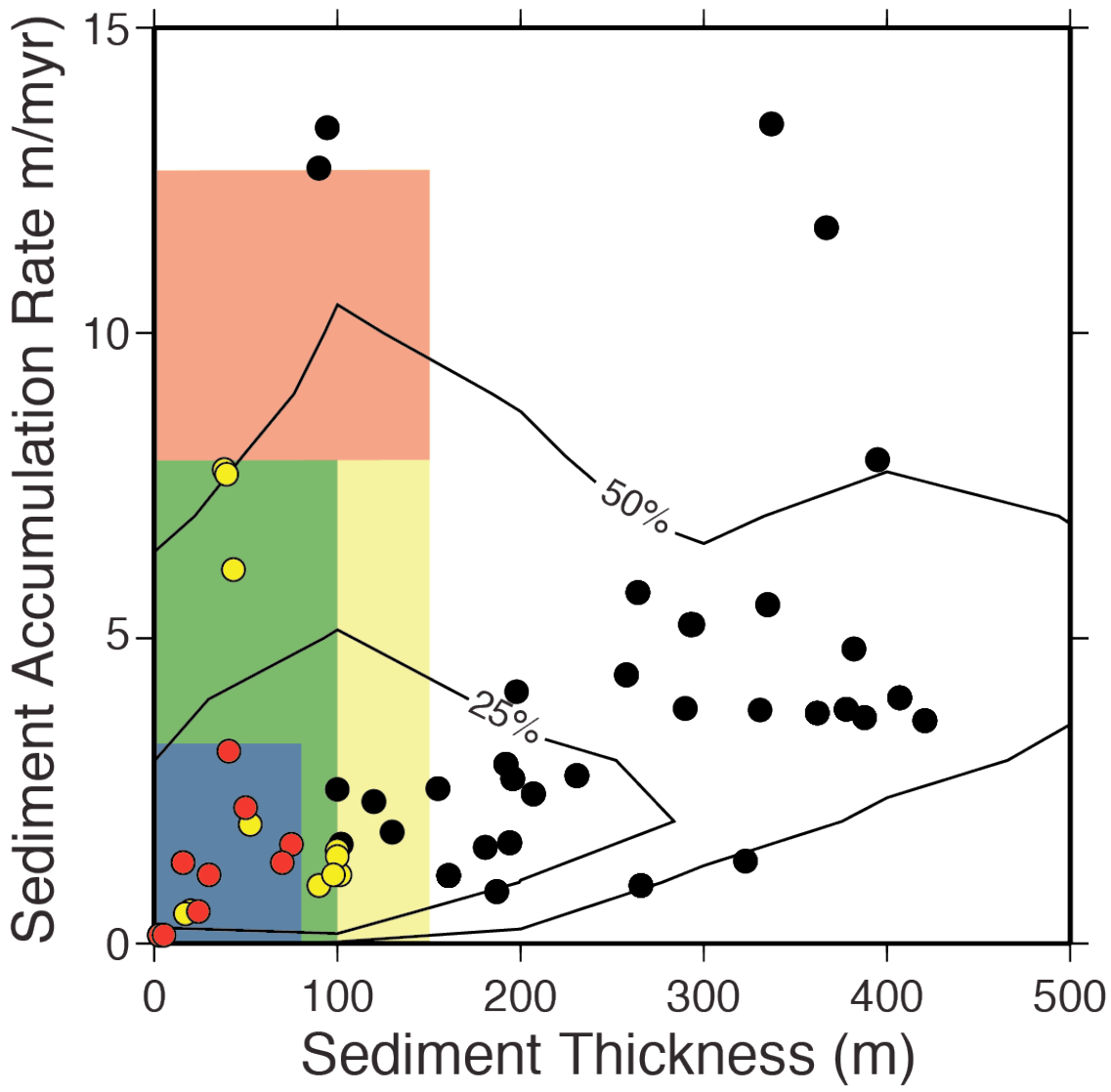

330

331

Fig 2B.